Protein Science (2000), *9*:1177–1193. Cambridge University Press. Printed in the USA.

The role of backbone conformational heat capacity in protein stability: Temperature dependent dynamics of the B1 domain of *Streptococcal* protein G

MICHAEL J. SEEWALD,[1] KUMAR PICHUMANI,[1] CHERI STOWELL,[1] BENJAMIN V. TIBBALS,[1] LYNNE REGAN,[2] AND MARTIN J. STONE[1]

[1]Department of Chemistry, Indiana University, Bloomington, Indiana 47405-0001
[2]Department of Molecular Biophysics and Biochemistry, Yale University, P.O. Box 208114, 266 Whitney Avenue, New Haven, Connecticut 06520-8114

(RECEIVED January 25, 2000; FINAL REVISION March 29, 2000; ACCEPTED March 30, 2000)

Abstract

The contributions of backbone NH group dynamics to the conformational heat capacity of the B1 domain of *Streptococcal* protein G have been estimated from the temperature dependence of ^{15}N NMR-derived order parameters. Longitudinal (R_1) and transverse (R_2) relaxation rates, transverse cross-relaxation rates (η_{xy}), and steady state $\{^1H\}-^{15}N$ nuclear Overhauser effects were measured at temperatures of 0, 10, 20, 30, 40, and 50 °C for 89–100% of the backbone secondary amide nitrogen nuclei in the B1 domain. The ratio R_2/η_{xy} was used to identify nuclei for which conformational exchange makes a significant contribution to R_2. Relaxation data were fit to the extended model-free dynamics formalism, incorporating an axially symmetric molecular rotational diffusion tensor. The temperature dependence of the order parameter (S^2) was used to calculate the contribution of each NH group to conformational heat capacity (C_p) and a characteristic temperature (T^*), representing the density of conformational energy states accessible to each NH group. The heat capacities of the secondary structure regions of the B1 domain are significantly higher than those of comparable regions of other proteins, whereas the heat capacities of less structured regions are similar to those in other proteins. The higher local heat capacities are estimated to contribute up to ~0.8 kJ/mol K to the total heat capacity of the B1 domain, without which the denaturation temperature would be ~9 °C lower (78 °C rather than 87 °C). Thus, variation of backbone conformational heat capacity of native proteins may be a novel mechanism that contributes to high temperature stabilization of proteins.

Keywords: B1 domain; entropy; heat capacity; NMR relaxation; order parameter; protein dynamics; protein stability

Most globular proteins are marginally stable because the factors that favor formation of the native state, primarily desolvation of hydrophobic groups and formation of intramolecular hydrogen bonds and salt bridges, are almost equally balanced against those that favor denaturation, primarily the higher conformational entropy of the unfolded protein chain relative to that of the native state (Creighton, 1993; Fersht, 1999). At high temperatures, the balance between these factors is altered such that many proteins exhibit reversible thermal denaturation with a characteristic midpoint, the melting temperature (T_m). The free energy of unfolding of a protein (ΔG_{N-U}) depends upon the changes in enthalpy, entropy, and heat capacity that occur upon unfolding and the temperature (T) according to the equation (Creighton, 1993; Fersht, 1999):

$$\Delta G_{N-U} = \Delta H_0 - T\cdot\Delta S_0 + \Delta C_{p,N-U}\cdot[T - T_0 - T\cdot\ln(T/T_0)] \quad (1)$$

in which ΔH_0 and ΔS_0 are the enthalpy and entropy changes, respectively, at a reference temperature T_0 and $\Delta C_{p,N-U}$ is the change in heat capacity at constant pressure, which is assumed to be invariant with temperature. Equation 1 indicates that native proteins may be stabilized by an increase in ΔH_0 or by a decrease in either ΔS_0 or $\Delta C_{p,N-U}$. Thus, one possible strategy for a protein to achieve high thermal stability is to increase the heat capacity of the native state, thereby decreasing $\Delta C_{p,N-U}$. The heat capacity of the native state of a protein may be partitioned into three major contributions resulting from fluctuations of primary (covalent) struc-

Reprint requests to: Martin J. Stone, Department of Chemistry, Indiana University, Bloomington, Indiana 47405-0001; e-mail: mastone@indiana.edu.

Abbreviations: CSA, chemical shift anisotropy; CPMG, Carr-Purcell-Meiboom-Gill; DSS, 2,2-dimethyl-2-silapentane-5-sulfonic acid; FID, free induction decay; HSQC, heteronuclear single quantum coherence spectrum; NOE, nuclear Overhauser effect; NOESY, nuclear Overhauser effect spectroscopy; PMSF, phenylmethylsulfonyl fluoride; RNase, ribonuclease; SSE, summed squared errors; T_1, longitudinal relaxation time constant; TOCSY, total correlation spectroscopy; η_{xy}, transverse cross-relaxation rate constant.

ture, of noncovalent interactions within the protein molecule, and of interactions of the protein molecule with solvent (including reorganization of solvent–solvent interactions) (Gomez et al., 1995). These terms have been estimated to contribute ~82, ~3, and ~15%, respectively, to the total heat capacity of folded proteins, although $\Delta C_{p,N-U}$ is largely dominated by changes in the solvation term (Gomez et al., 1995).

Although the total changes in thermodynamic parameters upon protein unfolding can be readily measured (e.g., by calorimetry), a more thorough understanding of the factors contributing to protein stability requires the thermodynamic contributions of various physical effects to be separated. Recent advances in the collection and analysis of NMR relaxation data have made it possible to estimate the contributions of individual bond vector fluctuations to conformational entropy and heat capacity (Akke et al., 1993; Li et al., 1996; Yang & Kay, 1996; Yang et al., 1997). The relaxation of protonated ^{15}N or ^{13}C nuclei in proteins is dominated by the angular fluctuations of the associated NH or CH bond vectors relative to the permanent magnetic field. Relaxation data can be analyzed according to the Lipari–Szabo model-free formalism to yield parameters describing the rotational diffusion of the whole molecule and the amplitudes and time scales of the internal motions of the NH or CH groups (Lipari & Szabo, 1982a, 1982b). The generalized order parameter (S^2) describes the amplitude of angularly restricted internal motion and is related to conformational entropy because both are derived from the same probability distribution of spatial coordinates (Akke et al., 1993). Thus, if a particular model is assumed for internal motions and if the motions of individual bond vectors are assumed to be independent from each other, the conformational entropy may be calculated from the order parameter (Yang & Kay, 1996). The heat capacity associated with bond vector fluctuations may then be estimated from the temperature dependence of the conformational entropy (Yang et al., 1997; Evenäs et al., 1999). These methods have been applied to estimate the contributions of backbone NH bond vector fluctuations to the heat capacity of the native calmodulin E140Q mutant C-terminal domain (Evenäs et al., 1999), the partially unfolded state of staphylococcal nuclease (Yang et al., 1997), and the unfolded state of the N-terminal SH3 domain from drk (Akke et al., 1998). In addition, the temperature dependence of NH order parameters of native ribonuclease H (RNase H) has been analyzed using an alternative formalism that yields a characteristic temperature reflecting the density of conformational states accessible to each NH group (Mandel et al., 1996). These previous studies suggest that the conformational heat capacity is typically relatively low for ordered secondary structured regions and higher for loops and terminal regions of folded proteins and for unfolded proteins.

In this paper, we describe an investigation of the contribution of backbone NH group conformational heat capacity to the thermal stabilization of a small protein domain, the B1 domain of Streptococcal protein G. The B1 domain is one of several highly conserved IgG binding domains in protein G, a cell surface protein that binds to the constant region of immunoglobulin allowing the bacteria to evade the host immune system (Bjorck & Kronvall, 1984; Akerstrom et al., 1985; Boyle, 1990; Fahnestock et al., 1990). The B1 domain (56 amino acid residues) is one of the smallest stable folded globular domains known and has been studied extensively by biophysical methods. The structure (Fig. 1), determined by both NMR spectroscopy and X-ray crystallography (Akerstrom et al., 1985; Gronenborn et al., 1991; Gallagher et al., 1994), consists of two β-hairpins (residues 1–20 and residues 42–56) that are associated to form a four-stranded mixed antiparallel/parallel β-sheet. A single α-helix (residues 22–37) lies across one face of the sheet. There are no proline residues or disulfide bonds. The B1 domain undergoes reversible thermal denaturation at ~87 °C (Gronenborn et al., 1991; Alexander et al., 1992a), yet its stability at physiologically relevant temperatures is not unusually high (Alexander et al., 1992a). The folding of the B1 domain has been studied extensively (Alexander et al., 1992b; Kuszewski et al., 1994; Orban et al., 1994, 1995; Kobayashi et al., 1995; Park et al., 1997; Blanco & Serrano, 1998; Sheinerman & Brooks, 1998) and the B1 domain has been used as a model system for the selection and design of modified hydrophobic core structures (O'Neil et al., 1995; Gronenborn et al., 1996; Dahiyat & Mayo, 1998), to test the secondary structure propensities of the amino acids (Minor & Kim, 1994a, 1994b; Smith et al., 1994;), to probe the influence of tertiary structural environment on secondary structure formation (Minor & Kim, 1996), and to evaluate the energetics of side-chain–side-chain interactions (Smith & Regan, 1995).

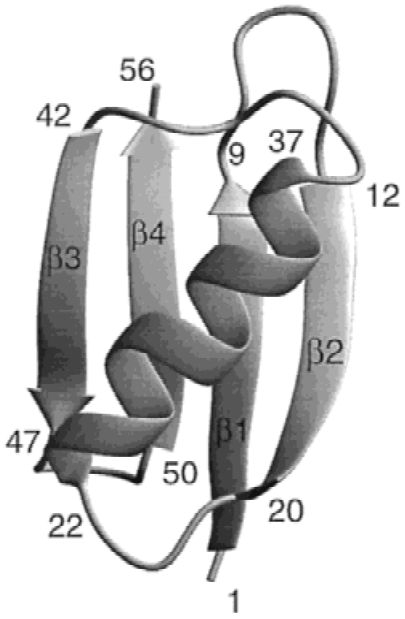

Fig. 1. Ribbon diagram showing the secondary structure of the B1 domain (Protein Data Bank accession code: 2gb1).

The backbone dynamics of the B1 domain have been determined previously for the native state at 26 °C (Barchi et al., 1994) and the urea-denatured state at pH 2 and 25 °C (Frank et al., 1995). The inner two β-strands of the native structure are very rigid, whereas the outer two strands and the turns and loops exhibit greater flexibility. Faster than average transverse relaxation of NH groups in the helix was attributed to slow fluctuations in the position of the α-helix relative to the β-sheet (Barchi et al., 1994). In the denatured state, the C-terminal β-hairpin sequence and the central and N-terminal regions of the α-helix sequence appear to be conformationally slightly more restricted than the remainder of the molecule (Frank et al., 1995).

In the current paper, we describe the backbone NH group dynamics of the native B1 domain at six temperatures over the range 0–50 °C. Cross-relaxation data and an anisotropic rotational diffusion model are used to separate the effects of molecular rotation and slow conformational exchange (Fushman & Cowburn, 1998).

The temperature dependence of backbone order parameters is used to calculate both local contributions to heat capacity and characteristic temperatures for each NH group and the results are compared to previous results for other proteins. We discuss the relevance of the backbone heat capacity to the high thermal stability of the B1 domain.

Results

Resonance assignments

The ^{1}H and ^{15}N assignments of the backbone NH groups of the B1 domain have been reported previously for 26 °C data (Barchi et al., 1994). In the present work, assignments have been extended to the temperatures 0, 10, 20, 30, 40, and 50 °C. In many cases, the NH assignments could be made readily by comparison with the published 26 °C spectrum (Barchi et al., 1994). Three-dimensional TOCSY-HSQC and NOESY-HSQC spectra were used to confirm assignments at 0, 20, and 50 °C. Assignments at the other temperatures were established by observation of smooth (nearly linear) variations of ^{1}H and ^{15}N chemical shifts across the 0–50 °C temperature range. For each temperature, it was possible to obtain assignments for all backbone NH groups. Few residues had to be excluded in the analysis of peak heights due to resonance overlap (10 °C: A24 and E42; 30 °C: Q2 and T55; 40 °C: Q2, T25, E27, Y33, E42, and T55; 50 °C: T25 and E27). ^{1}H and ^{15}N temperature coefficients (the slope of the linear chemical shift vs. temperature plots) were calculated for each residue (data not shown). The temperature coefficients do not correlate significantly with the solvent accessible surface areas (SASA) of the corresponding NH groups, as determined from the average energy minimized NMR structure (Gronenborn et al., 1991); r^2 values are 0.26 and 0.02, respectively, for ^{1}H and ^{15}N temperature coefficients.

Relaxation parameters

Relaxation parameters (R_1, R_2, NOE, and η_{xy}) and their uncertainties were determined from the peak heights as described in Materials and methods. The values of the relaxation parameters are presented graphically in Figure 2; the data and uncertainties are also listed in the Supplementary material in the Electronic Appendix. The 10% trimmed weighted average values of R_2 and the NOE (Table 1) both decrease with increasing temperature, as expected for an increased density of fast time scale motions at higher temperature. The 10% trimmed weighted average value of R_1 (Table 1) increases gradually from 0 to 30 °C then decreases again at the higher temperatures. This classical behavior for longitudinal relaxation rates (Sanders & Hunter, 1987) reflects the fact that the spectral density function at the nitrogen Larmor frequency $J(\omega_N)$ is maximum at 30 °C; this trend was confirmed by reduced spectral density mapping (data not shown) (Farrow et al., 1995).

Anisotropic rotational diffusion and exchange broadening

The principal moments of inertia of the NMR structure (Gronenborn et al., 1991) of the B1 domain are in the ratio 1.00:0.90:0.52, suggesting that rotational diffusion of the domain is significantly anisotropic. The dimensions and orientation of an anisotropic or axially symmetric diffusion tensor may be readily estimated from the ^{15}N R_2/R_1 ratios and the known structure of the molecule (Tjandra et al., 1995). The R_2/R_1 ratios for all residues at each temperature are shown in Figure 2D. At the low temperatures, residues in the α-helix clearly have higher R_2/R_1 ratios than the rest of the molecule and there are several other residues with higher than typical values (e.g., residues 48 and 49 at 0 °C). At 40 and 50 °C, the difference between R_2/R_1 ratios for the α-helix and the rest of the molecule is much less prominent, but there are still several isolated residues displaying elevated values. The observed variation in R_2/R_1 may be influenced by several factors. First, if molecular tumbling is anisotropic, NH groups pointing along the long axis of the molecule will reorient more slowly than other NH groups, resulting in elevated R_2/R_1 ratios. Second, NH groups influenced by chemical or conformational exchange on the microsecond to millisecond timescale will have increased R_2/R_1 ratios, due to an exchange broadening (R_{ex}) contribution to R_2. Third, aggregation of protein molecules would lead to slower tumbling, hence increased R_2/R_1 ratios. Although the latter effect is most likely to influence all NH groups equally, there may be some selective influences on certain residues depending on the structures and symmetry of the aggregates. We performed several analyses to separate these possible effects and to investigate whether there were any significant differences in the anisotropy of molecular rotational diffusion at the different temperatures.

To investigate whether aggregation was occurring, the R_1 and R_2 experiments were repeated with a threefold diluted (0.9 mM) sample at 50 °C. The average R_2/R_1 ratio did not change significantly (data not shown), providing evidence that aggregation was not occurring.

To identify residues whose transverse relaxation rates are influenced by exchange on the microsecond to millisecond timescale, we compared the ratio of the transverse auto-relaxation rate (R_2) to the transverse cross-relaxation rate (η_{xy}) across the protein (see Materials and methods). Results obtained for η_{xy} and the ratio R_2/η_{xy} are shown in Figures 2E and 2F; η_{xy} values are listed in the Supplementary material in the Electronic Appendix. At each temperature, the R_2/η_{xy} ratio is approximately constant for all residues, indicating that most residues are not influenced by exchange broadening. The 10% trimmed weighted average values of η_{xy} (Table 1) decrease gradually with increasing temperature (0 and

Table 1. *Average relaxation and dynamics parameters*

	10% trimmed weighted average of					
	0 °C	10 °C	20 °C	30 °C	40 °C	50 °C
R_1	1.90	2.20	2.30	2.35	2.13	1.93
R_2	8.54	6.35	5.38	4.32	3.70	3.23
NOE	0.75	0.72	0.67	0.55	0.42	0.27
R_2/R_1	4.36	2.91	2.34	1.84	1.72	1.60
η_{xy}	5.69	4.23	3.34	2.72	2.23	1.87
R_2/η_{xy}	1.47	1.57	1.54	1.59	1.63	1.67
S_f^2	0.85	0.78	0.77	0.73	0.65	0.60
S^2_{total}	0.85	0.77	0.76	0.71	0.63	0.54
τ_f (ps)	19.4	24.5	25.3	39.6	49.6	57.9
R_{ex}	0.46	0.41	0.30	0.26	0.32	0.47
Cone semi-angle from S_f^2	18.5	23.1	24.0	25.9	30.1	32.9
Cone semi-angle from from S^2_{total}	18.9	23.5	24.2	26.9	31.1	35.9

50 °C values differ by a factor of ~3.0), following the same trend as seen for R_2 data. Interestingly, the 10% trimmed weighted average values of R_2/η_{xy} (Table 1) increase slightly with temperature (by ~14% from 0 to 50 °C). This increase is most likely to result from either an increase in exchange broadening contributions at higher temperatures or an increase in high frequency spectral densities at higher temperatures reducing the validity of the assumption underlying Equation 3. However, we cannot rule out the

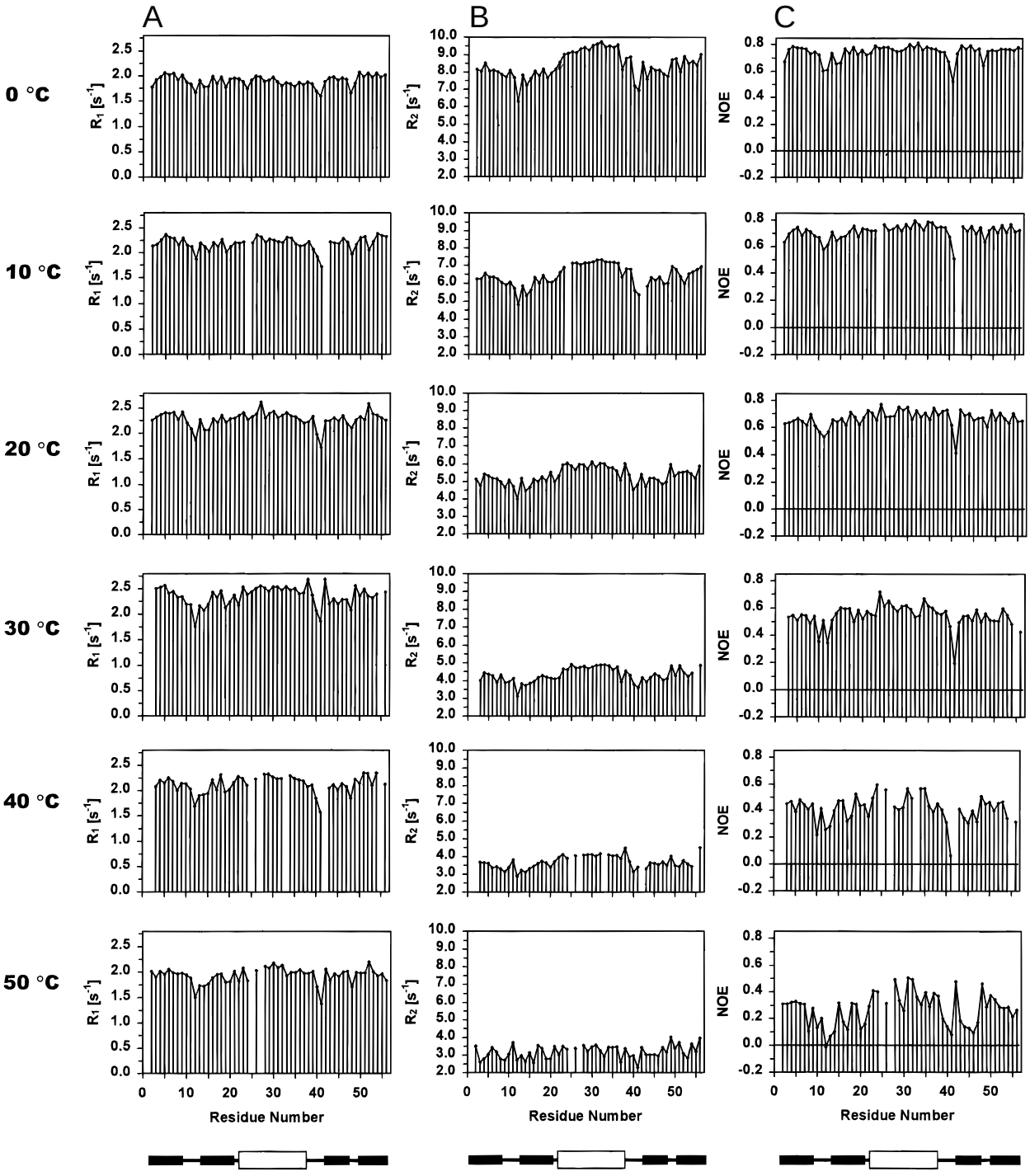

Fig. 2. Relaxation parameters plotted vs. residue number at all six temperatures. Data at 0, 10, 20, 30, 40, and 50 °C are arranged from top to bottom. **A:** Longitudinal relaxation rate constants R_1. **B:** Transverse relaxation rate constants R_2. **C:** Steady-state $\{^1H\}-^{15}N$ NOEs. **D:** R_2/R_1 ratios. **E:** Transverse cross-relaxation rate constants η_{xy}. **F:** R_2/η_{xy} ratios. Values and uncertainties are listed in the Supplementary material in the Electronic Appendix. The positions of the β-strands and the α-helix are indicated schematically at the bottom by solid and open rectangles, respectively. (*Figure continues on facing page.*)

possibility that variations in R_2/η_{xy} with temperature reflect differences in the NH bond length, chemical shift anisotropy, and/or angles between principal axes of CSA and dipolar tensors.

Despite the relatively flat distributions of R_2/η_{xy} values at each temperature, several residues show R_2/η_{xy} values clearly above the average (Fig. 2F). After exclusion of those residues with large amplitude fast internal motions (NOE $\leq$ 0.3), we applied the criterion that the R_2/η_{xy} value of a given residue exceeds the average ratio at that temperature by more than one standard deviation to identify the following residues as being subject to conformational exchange: T11, G14, G41, Y45, T49, and F52 (0 °C); G14, G41, T49, and F52 (10 °C); G41, T49, and T53 (20 °C); T11, T49, T51, T53, and E56 (30 °C); T11, K13, G38, T49, F52, and E56 (40 °C); and I6, E15, T18, G38, and T51 (50 °C). Notably, none of the

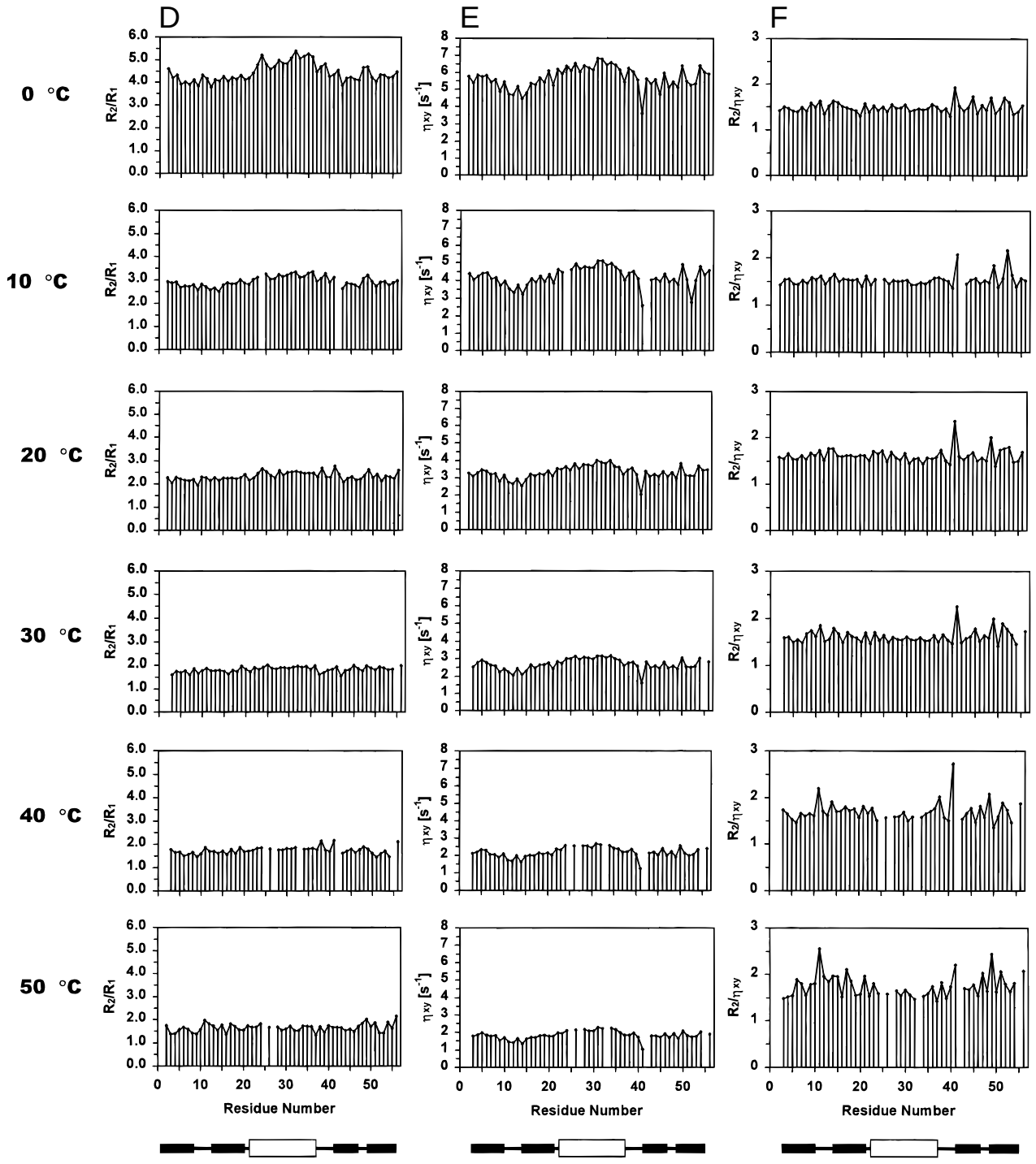

Fig. 2. *Continued.*

Table 2. *Molecular rotational diffusion parameters*

Diffusion parameter	0 °C	10 °C	20 °C	30 °C	40 °C	50 °C	Weighted average
$D_{\parallel}/D_{\perp}$ [a]	1.34 ± 0.04	1.25 ± 0.04	1.26 ± 0.04	1.23 ± 0.06	1.27 ± 0.10	1.37 ± 0.23	1.27
θ (deg) [a]	85 ± 3	71 ± 9	80 ± 6	85 ± 10	95 ± 10	61 ± 24	83.81
φ (deg) [a]	182 ± 6	186 ± 8	176 ± 9	191 ± 12	205 ± 10	180 ± 12	185.20
τ_m (ns) [a]	7.00	5.18	4.17	3.22	2.98	2.84	—
τ_m (ns) [b]	7.03	5.19	4.19	3.21	2.94	2.63	—
η_{buffer} (mPa s)	1.80	1.34	1.04	0.84	0.70	0.60	—
τ_m/η_{buffer} [b] (10^{-6}/Pa)	3.90	3.86	4.02	3.81	4.20	4.42	—

[a] These parameters were determined separately from the R_2/R_1 ratios at each temperature using the program quadric diffusion.
[b] These τ_m values were determined at each temperature to be optimally consistent with weighted average values of $D_{\parallel}/D_{\perp}$, θ, and φ. These values were used for model-free calculations.

selected residues is in the α-helix. For most of these residues, the elevated R_2/η_{xy} ratios are clearly caused by high R_2 values. However, a small number of residues (e.g., G14 and G41) show high R_2/η_{xy} values that are apparently caused by low η_{xy} values. These residues may experience internal motion that is not accounted for in the derivation of Equation 3.

The dimensions and orientation of the rotational diffusion tensor were estimated from weighted mean R_2/R_1 ratios at each temperature for residues not exhibiting large amplitude fast internal motions or exchange broadening (Tjandra et al., 1995). The data for each temperature were fitted to each of four rotational diffusion models: fully anisotropic [$D_{xx} \neq D_{yy} \neq D_{zz}$]; prolate axially symmetric [D_{zz} ($\equiv D_{\parallel}$) > $D_{xx} = D_{yy}$ ($\equiv D_{\perp}$)], oblate axially symmetric [D_{zz} ($\equiv D_{\parallel}$) < $D_{xx} = D_{yy}$ ($\equiv D_{\perp}$)], and fully isotropic diffusion [$D_{xx} = D_{yy} = D_{zz}$]. F-statistical analysis was used to select the most appropriate model (Tjandra et al., 1995). At all temperatures: (1) the improved agreement with the experimental data observed for the prolate axially symmetric model relative to the isotropic model is statistically significant ($p < 0.05$) (Tjandra et al., 1995); (2) the improved agreement with the experimental data observed for the fully anisotropic model relative to the prolate axially symmetric model is not statistically significant ($p > 0.05$); and (3) the fully anisotropic tensor calculations support the prolate model. Based on χ^2 comparisons, the prolate axially symmetric model is superior to the oblate axially symmetric model at all temperatures except 50 °C (Blackledge et al., 1998). However, even at 50 °C, χ^2 differs by only 6% for these two models, and the diffusion components for the fully anisotropic model are most consistent with a prolate tensor (D_{zz}:D_{xx}:D_{yy} = 1.34:1.04:1). Based on these considerations, and in the interest of maintaining consistency between the data sets at each temperature, we chose to analyze all data sets using a prolate axially symmetric diffusion model. Initial estimates of the effective overall correlation time [$\tau_m = (2D_{\parallel} + 4D_{\perp})^{-1}$], the ratio of unique and perpendicular components of the diffusion tensor ($D_{\parallel}/D_{\perp}$), and the angles defining the position of the unique axis (θ and φ) are listed in Table 2. As expected, the effective correlation time decreases with increasing temperature. However, the dimensions and orientation of the diffusion tensor change only very slightly across the observed temperature range. Since the magnitude of the variation is not much larger than the estimated uncertainties, we considered it reasonable to perform subsequent calculations under the assumption that the parameters $D_{\parallel}/D_{\perp}$, θ, and φ are identical at all temperatures. The weighted average values of those determined at the individual temperatures (Table 2) were used in subsequent calculations along with the τ_m values optimally consistent with these $D_{\parallel}/D_{\perp}$, θ, and φ values and the R_2/R_1 ratios at each temperature (Table 2). The optimized τ_m values correlate well with the calculated buffer viscosity (η_{buffer}) at each temperature ($r^2 = 0.995$) as expected from the Stokes–Einstein relationship; thus, the τ_m/η_{buffer} ratios (Table 2) are approximately constant.

Model free dynamics

Five models, described in Materials and methods, were used to appropriately fit the dynamics parameters to the experimental relaxation data. A summary of the models selected is given in Table 3. The optimized dynamics data are displayed in Figure 3 and listed in the Supplementary material in the Electronic Appendix.

At most temperatures, the regions of the B1 domain that exhibit the lowest order parameters are the β1–β2 type I hairpin turn, including part of the β2-strand (residues 10–14), and the extended loop between the α-helix and strand β3 (residues 39–41). Interestingly, all four glycine residues in the B1 domain (G9, G14, G38, and G41) are located immediately preceding or at the C-terminal ends of these two flexible regions, suggesting that the glycines may act as hinges to allow these regions to move somewhat independently from the rest of the domain. The order parameters of the N- and C-termini are comparable to the weighted average for the whole domain, indicating that these regions are unusually rigid. In

Table 3. *Model selection statistics* [a]

	Number of residues fit to					
	0 °C	10 °C	20 °C	30 °C	40 °C	50 °C
Model 1 (S_f^2)	10	17	4	1	0	0
Model 2 (S_f^2, τ_f)	18	26	34	33	34	32
Model 3 (S_f^2, R_{ex})	2	0	3	0	0	0
Model 4 (S_f^2, τ_f, R_{ex})	14	5	8	11	11	16
Model 5 (S_f^2, S_s^2, τ_s)	11	5	6	8	4	5

[a] Shown is the number of residues fit to each of the five dynamics models at each temperature.

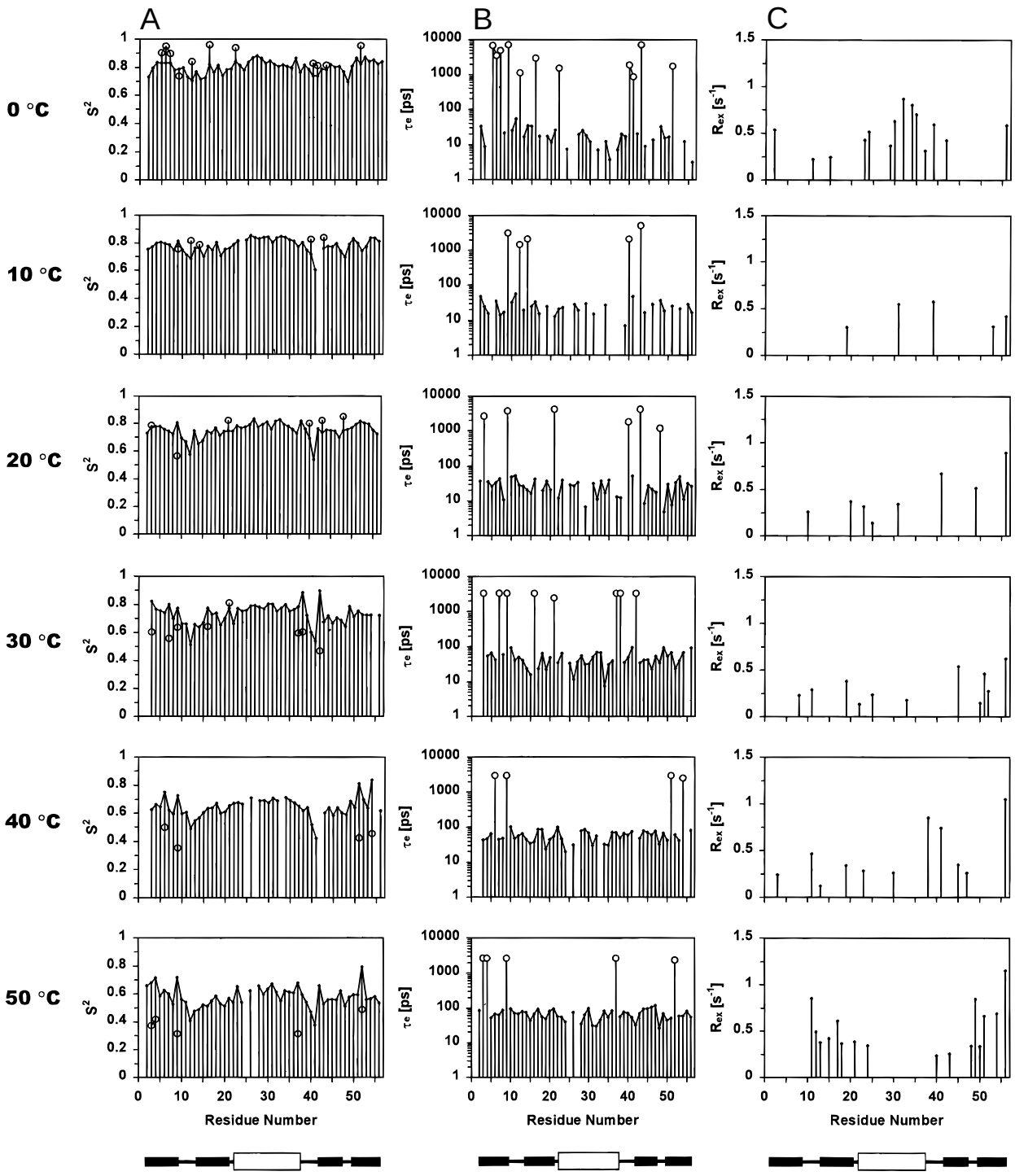

Fig. 3. Model-free dynamics parameters plotted vs. residue number at all six temperatures. Data at 0, 10, 20, 30, 40, and 50 °C are arranged from top to bottom. **A:** Order parameters on fast and slow timescales S_f^2 (●) and S_s^2 (○), respectively. **B:** Internal correlation times on fast and slow timescales τ_f (●) and τ_s (○), respectively. **C:** Conformational exchange terms R_{ex}. Values and uncertainties for all parameters are listed in the Supplementary material in the Electronic Appendix. The positions of the β-strands and the α-helix are indicated schematically at the bottom by solid and open rectangles, respectively.

the α-helix (residues 22–37), order parameters are fairly uniform and slightly higher than in adjacent regions. Small but systematic differences in order parameters are observed between the different strands in the β-sheet at all temperatures studied. The most flexible strand is β_2, followed by β_3; the inner two β-strands of the sheet (β_1 and β_4) are significantly more rigid.

Internal correlation times are required to obtain adequate fits for the majority of residues (Table 3). The 10% trimmed weighted

average fast internal correlation times (τ_f) increase with increasing temperature (Table 1). Although a decrease in the rates of internal motions is at first surprising, it may be correlated with the observed temperature dependent increases in the amplitudes of these motions (Farrow et al., 1997), i.e., larger amplitude motions are generally slower.

Order parameters and correlation times describing a second timescale of subnanosecond internal motions (model 5) are required to adequately fit the relaxation data for a few residues (4–11) at each temperature. Although the selection of residues exhibiting such motions is not consistent between temperatures, it is noteworthy that none of these residues is located in the central region of the α-helix (residues 23–36). It has been noted previously that τ_s values should be interpreted with caution because of their limited precision (Stone et al., 1993; Jin et al., 1998).

Exchange broadening terms are required to obtain appropriate fits for 5 to 16 residues at each temperature (Table 3). However, in all cases the exchange parameters are small ($<1.2\ s^{-1}$) and the residues that require these terms are generally not consistent between temperatures. The only residues that exhibit exchange broadening at three or more consecutive temperatures are T11 in the type I turn and the C-terminal residue, E56. The R_{ex} terms of both these residues increase over the 30 to 50 °C temperature range. Such an increase would be expected if the timescale of exchange kinetics approaches the timescale of the CPMG refocusing period (1 ms) as the temperature is increased (Palmer et al., 1996). This would suggest that the R_{ex} terms observed for T11 and E56 result from motions on a timescale slower than 1 ms. However, an alternative explanation is that the thermally induced change in relative populations of the two exchanging states gives rise to the increase in R_{ex} (Palmer et al., 1996); model calculations indicate that the latter mechanism could readily account for the modest increases observed in the current study.

Temperature dependence of order parameters

Order parameters in the B1 domain decrease as the temperature is increased (Fig. 3A; Table 1). The present calculations do not assume any particular motional model. However, the data may be arbitrarily represented by the "diffusion in a cone" model, where the order parameter is indicative of the cone semi-angle (Lipari & Szabo, 1980, 1981; Clore et al., 1990a). The trimmed weighted average cone semi-angles calculated from S^2 values at each temperature are listed in Table 1. The increase of only ~17° in cone semi-angle suggests that the factors restricting the local motions of most NH groups do not change significantly over the 0–50 °C temperature range. This is consistent with the B1 domain maintaining its folded globular structure up to significantly greater than 50 °C (Gronenborn et al., 1991; Alexander et al., 1992a).

The temperature variation of the order parameters was analyzed according to Equations 5–7 to yield local heat capacities (C_p) and characteristic temperatures (T^*) for each backbone NH vector in the B1 domain (Mandel et al., 1996; Yang & Kay, 1996; Yang et al., 1997). Plots of entropy (S_B) vs. $\ln(T)$, used to determine local heat capacities (Equation 6), were approximately linear for most residues; examples are shown in Figure 4A. Squared correlation coefficients (r^2; Fig. 5A) exceeded 0.7 for 87% and 0.8 for 66% of residues. Similarly, plots of $1 - S$ against temperature were approximately linear for most residues over the 0–50 °C range, allowing T^* values to be readily determined (Equation 7); examples are shown in Figure 4B. Squared linear correlation coefficients (Fig. 5B) exceeded 0.7 for 80% and 0.8 for 62% of NH groups.

In the fits used to determine either C_p or T^* values, the lack of linearity for residues with $r^2 \leq 0.70$ could usually be attributed to the relaxation data having been fit to dynamics model 5 (describing two timescales of internal motions) at some temperatures but to different models at other temperatures. Nevertheless, performing the above fits using the fast timescale order parameters (S_f) rather than the generalized order parameters did not generally improve the quality of the fits or significantly alter the T^* or C_p values obtained (data not shown). For the purposes of studying the temperature dependence of order parameters, it would be ideal to fit each residue to the same dynamics model at all six temperatures. However, imposing our model selection criteria independently at each temperature resulted in only five residues in the B1 domain being fit to the same model at all temperatures. To investigate the degree to which model variation was influencing the quality of the fits observed, we calculated C_p and T^* values from dynamics data in which all residues were constrained to the same model (model 2) at all temperatures. Model 2 was chosen because it is the most frequently selected model at all five temperatures (Table 3). Although this procedure resulted in a noticeable improvement in the fits (all residues now had r^2 values greater than 0.7), the C_p and T^* values calculated from data limited to model 2 showed similar trends to those found using data calculated from different dynamics models at different temperatures (data not shown). Furthermore, limiting all residues to model 2 is somewhat artificial because model 2 clearly does not appropriately account for the observed relaxation properties of many residues. Therefore, we present here (Fig. 5C,D) the C_p and T^* values calculated using variable models at different temperatures, but we omit the data points for which the fits were nonlinear (arbitrarily chosen as $r^2 \leq 0.70$).

Discussion

Comparison with previous dynamics results

We have characterized the internal dynamics of the protein G B1 domain at six temperatures. The dynamics of the native B1 domain have been previously characterized by Barchi et al. (1994) at 26 °C. In general the previous relaxation and dynamics parameters follow similar trends to those observed for the present data at 20 and 30 °C. In particular, the same two regions displayed the lowest order parameters. Small differences between the order parameter values in the previous and current studies can most likely be attributed to either: (1) the use of an anisotropic tumbling model in the current study and an isotropic tumbling model in the previous study; (2) different model selection methods; or (3) the slight temperature difference between the two studies.

The most significant difference between the current and previous results is that Barchi et al. (1994) identified the whole α-helix as having slow motions (R_{ex} terms), whereas we have found these terms to be very small or absent for helical residues above 0 °C. Barchi et al. concluded that the α-helix undergoes a rigid body rotational motion relative to the underlying sheet. This conclusion was consistent with an ~8–10° difference in the relative orientations of the helix and sheet between the NMR and X-ray structures (Gronenborn et al., 1991; Achari et al., 1992; Gallagher et al., 1994). In contrast, the current data do not provide evidence for such reorientation. The differences between the helix R_{ex} values found in the present and previous studies can be attributed to the

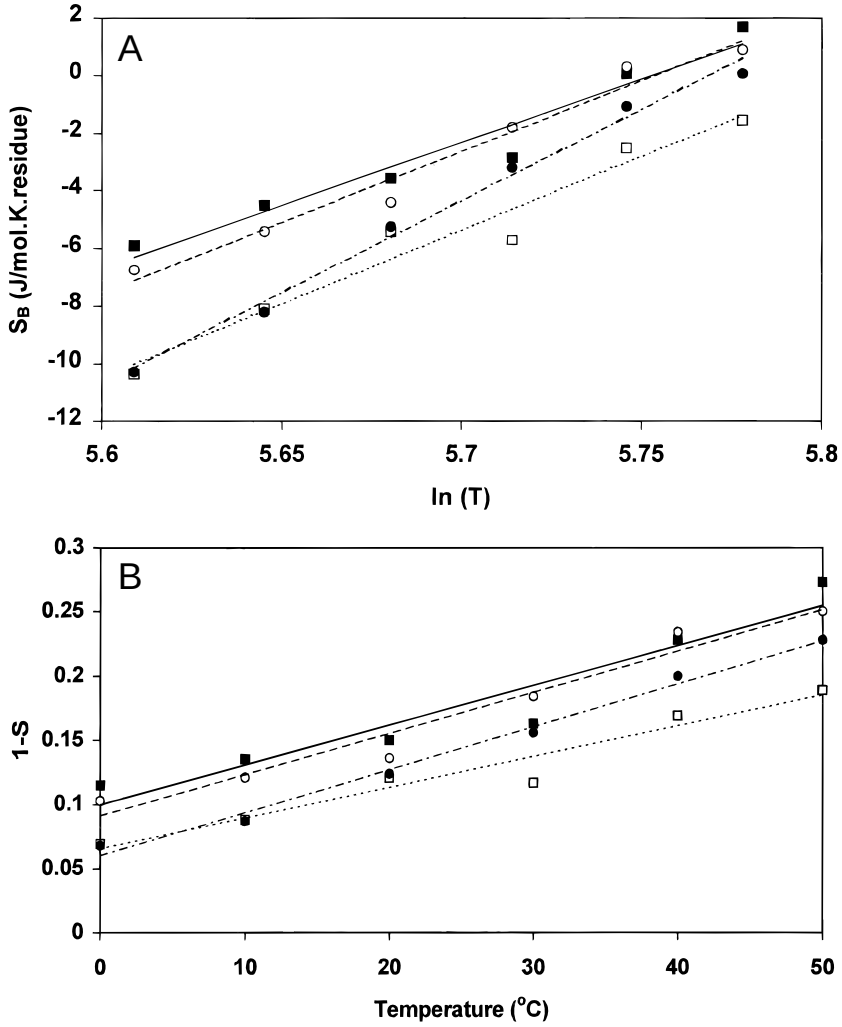

Fig. 4. A: Plots of the estimated Boltzmann entropy (S_B) vs. the natural logarithm of the temperature ($\ln(T)$) for residues N8 (■), K28 (□), Y45 (○), and K50 (●). Linear least-squares fits of the data are shown as N8 (solid line), K28 (dotted line), Y45 (dashed line), and K50 (dashed-dotted line). Squared linear correlation coefficients (r^2) are 0.95 (N8), 0.96 (K28), 0.97 (Y45), and 0.99 (K50). **B:** Plots of $(1 - S)$ vs. temperature for residues N8 (■), K28 (□), Y45 (○), and K50 (●). Linear least-squares fits of the data are shown as N8 (solid line), K28 (dotted line), Y45 (dashed line), and K50 (dashed-dotted line). Squared linear correlation coefficients (r^2) are 0.91 (N8), 0.95 (K28), 0.96 (Y45), and 0.99 (K50).

use of an anisotropic tumbling model in the present study and an isotropic model in the previous study. In the current study, NH groups in the helix clearly exhibit high transverse relaxation rates and consequently high R_2/R_1 ratios (Fig. 2D), as observed in the previous study (Barchi et al., 1994). If the data are analyzed with the assumption that the molecule is tumbling isotropically then the only way to account for the high R_2 values is to incorporate an exchange broadening term for these residues. Alternatively, if an anisotropic diffusion tensor is used, then an elevated R_2 value may be attributed either to exchange broadening or to orientation of the NH vector along the long axis of the molecule. The cross-relaxation measurements made in this study (Fig. 2E,F) allowed us to differentiate between these two effects. We found that high R_2 values occur in the α-helix primarily because all the helix NH groups are aligned relatively closely with the long axis of the molecule, resulting in slower reorientation of these NH vectors compared to most other NH groups in the molecule. The unique axis of the diffusion tensor and the long axis of the α-helix are separated by an angle of $\sim$33°, whereas NH groups in the β-sheet make angles of $\sim$60–120° with the unique axis (average angle = 92°; standard deviation = 16°). It appears likely that analysis of the data of Barchi et al. using an anisotropic diffusion model would lead similarly to the elimination or reduction of many of the R_{ex} terms. A similar effect has been found for an α-helix in RNase H (Kroenke et al., 1998). This comparison emphasizes the importance of experiments that allow conformational exchange effects to be distinguished from the effects of anisotropic rotational diffusion.

Heat capacities and characteristic temperatures

Several previous NMR relaxation studies have investigated the temperature dependence of high frequency motions of protein backbone amide groups. In several of these cases (Bhattacharya et al., 1999; Bracken et al., 1999; Jin & Liao, 1999; Meekhof & Freund,

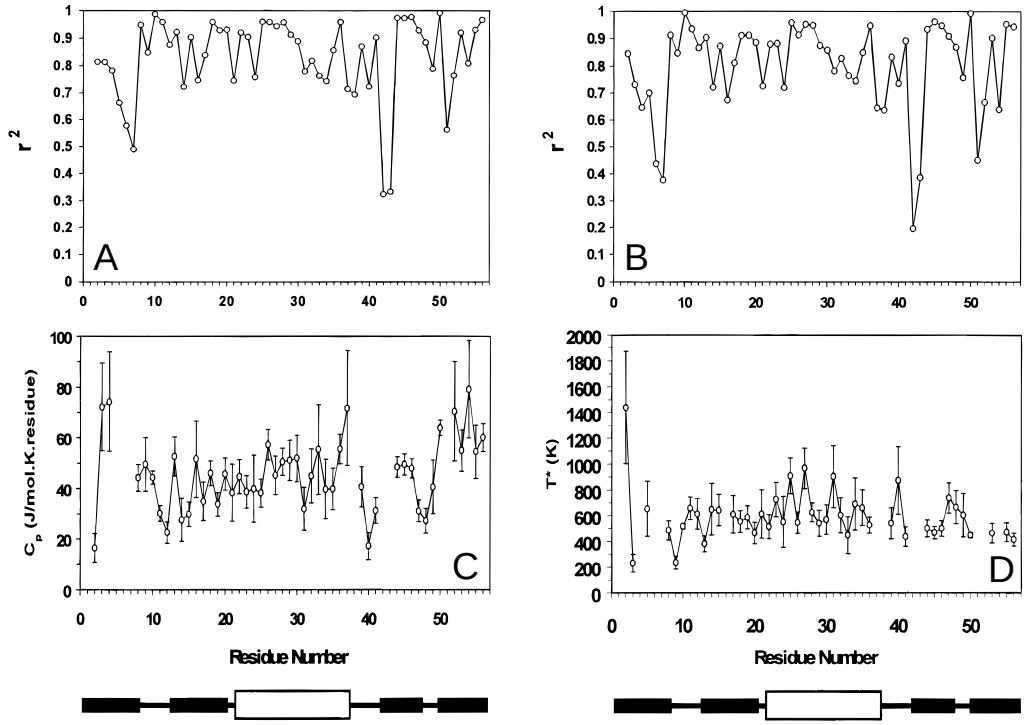

Fig. 5. Squared correlation coefficients (r^2) of the linear fits used to determine **(A)** C_p values and **(B)** T^* values for each residue. (**C**) Plot of heat capacity (C_p) vs. residue number. (**D**) Plot of characteristic temperature (T^*) vs. residue number. C_p and T^* are shown only for the residues for which r^2 exceeds 0.70. The positions of the β-strands and the α-helix are indicated schematically at the bottom by solid and open rectangles, respectively.

1999), the data could not be fit to the model free formalism over the temperature ranges studied, either because the protein of interest was largely unstructured or because the dynamics were more complex than the model free formalism allows. For these proteins, the data were usually analyzed by the reduced spectral density mapping approach (Farrow et al., 1995). For the dimer of the coiled coil transcription factor GCN4, the variation of the high frequency spectral density $J(0.87\omega_H)$ with temperature was fit to a straight line; the slope was positive for the unstructured basic region but close to zero for the structured helical region of the protein (Bracken et al., 1999). The current data are somewhat unusual in that the model-free approach fits the relaxation data well over the large range of temperatures used. This may be a reflection of the high thermal stability of the B1 domain and the absence of significant slow timescale motions over the 0–50 °C temperature range. We know of three previous studies focusing on the variation of NH group order parameters with temperature (Mandel et al., 1996; Yang et al., 1997; Evenäs et al., 1999). For RNase H (Mandel et al., 1996), the variation was described in terms of a characteristic temperature (T^*) for each NH group. T^* is a measure of the density of energy states accessible to the NH group upon an increase in temperature (in the temperature range studied). Thus, if $T^*/T = 1$ a temperature increase allows access to many additional conformational states, whereas if $T^*/T \gg 1$ few additional states are accessible upon a temperature increase. For the unfolded states of a staphylococcal nuclease mutant (Δ131 Δ) and the N-terminal SH3 domain of drk (Yang et al., 1997) and for the folded E140Q mutant of the calmodulin C-terminal domain (Evenäs et al., 1999), the order parameters were used to estimate the entropy of each NH group at each temperature and the temperature variation of the entropy was used to calculate the local heat capacity (C_p). We have analyzed the B1 domain data using both of the previously suggested methods to allow quantitative comparison of the present data (Fig. 5) to those observed for other globular proteins.

Heat capacity and characteristic temperature statistics for β-sheet, α-helix, and other residues in the B1 domain are listed in Table 4, along with comparative data for other proteins (Mandel et al., 1996; Yang et al., 1997; Evenäs et al., 1999). Within the B1 domain there is only a weak influence of secondary structure on the local heat capacity. In contrast, the previous studies of the E140Q calmodulin domain and RNase H have found flexible structures to have significantly higher heat capacities (or lower characteristic temperatures) than regular secondary structures. The C_p (or T^*) values of B1 domain residues not located in the α-helix or the β-sheet are generally similar to those for comparable regions of other folded proteins and to the values obtained for unfolded proteins. In contrast, the secondary structure regions of the B1 domain have substantially higher heat capacities than the secondary structures of the calmodulin domain mutant and dramatically lower characteristic temperatures than the secondary structure regions of RNase H. This indicates that the motions of NH groups in the secondary structures of the B1 domain undergo substantially greater increases in flexibility in response to temperature than corresponding groups in the other two proteins.

We have also searched for correlations between the backbone heat capacities for B1 domain residues and other structural parameters. The C_p and T^* values do not correlate with the solvent

Table 4. *Comparison of C_p and T* for the B1 domain and other proteins*

Protein	Temperatures (°C)	Structural element	C_p (J/mol·K·residue)	T^* (K)[a]	References
B1 domain	0, 10, 20, 30, 40, 50	All residues	46 (14)	596 (201)	
		All residues (10% trimmed)	45 (12)	584 (125)	
		β-Sheet	49 (17)	573 (265)	
		α-Helix	47 (10)	652 (160)	
		Other residues	37 (13)	573 (157)	
RNase H	12, 27, 37	Secondary structures		~3,700	Mandel et al. (1996)
		Flexible regions		~400 to ~900	
Calmodulin domain E140Q mutant	18, 28, 35	Secondary structures	~0–15		Evenäs et al. (1999)
		Linker (loop)	~20		
		Termini	~40		
Drk SH3 domain (guanidine denatured)	5, 14, 30	All residues	34 (10)		Yang et al. (1997)
Δ131ΔS nuclease (partially unfolded)	15, 32	All residues	59 (17)		Yang et al. (1997)

[a]Shown are the average values of the C_p and T^* values, with standard deviations given in parentheses.

accessible surface area (SASA) of the NH groups, the absolute or relative SASA of the whole amino acid, or the ^{1}H or ^{15}N temperature coefficients calculated from the chemical shifts; in all cases these correlations have r^2 values less than 0.2. In the region from residue ~15 to ~27, alternate residues display increasing and decreasing C_p or T^* values, whereas residues ~27 to ~37 display a periodicity of three to four residues. Although this pattern initially seems to indicate a change from β-strand to α-helix periodicity, the transition occurs around residue 27, whereas the helix begins at residue 22, and the C_p and T^* values in these regions do not correlate with surface exposure of NH groups or side chains.

From a structural viewpoint, NH groups with high heat capacities or low characteristic temperatures are likely to have relatively few interactions restricting their flexibility; thus, a temperature increase would readily overcome these interactions allowing access to a wide range of conformations. Therefore, the current data suggest that the motions of NH groups in the B1 domain secondary structures are limited by a small number of interactions in comparison to NH groups in the structured regions of the calmodulin domain and RNase H (Mandel et al., 1996; Evenäs et al., 1999). A possible trivial explanation of our observation is that the current study covers a much wider temperature range (50 °C) than the previous studies (maximum previous range was 25 °C for RNase H) and that the variation of order parameters is accentuated by the inclusion of data for the more extreme temperatures. Arguing against this explanation are the observations that (1) heat capacity values calculated using only 10–30 °C data are not systematically different from those calculated from data at all six temperatures; and (2) plots used to determine C_p or T^* were approximately linear over the whole 50 °C temperature range (Fig. 4). An alternative possibility is that the mobility of NH groups in the regular structural elements of the B1 domain is more sensitive to temperature because the core of the B1 domain is smaller than those of the other proteins. The B1 domain, calmodulin domain, and RNase H have 56, 71, and 152 amino acids, respectively, and folding of these domains is estimated to bury ~4,900, ~5,600, and ~15,400 Å^2 of protein surface area, respectively. Thus, the size difference seems adequate to account for the observed heat capacity differences of the B1 domain from RNase H, but is unlikely to account for differences from the calmodulin domain.

Influence of heat capacity on thermal stability

The high backbone heat capacities of the B1 domain secondary structural elements may contribute to the difference in thermal denaturation temperatures (T_m) of the B1 domain (87 °C) (Alexander et al., 1992a) and RNase H (66 °C)(Hollien & Marqusee, 1999); the T_m and folding thermodynamics of the E140Q calmodulin domain have not been reported. The thermal stability profiles of the B1 domain and RNase H are shown in Figure 6 (Alexander et al., 1992a; Hollien & Marqusee, 1999). Although these two proteins have similar free energies of unfolding in the 0–50 °C temperature range, their stabilities differ significantly at

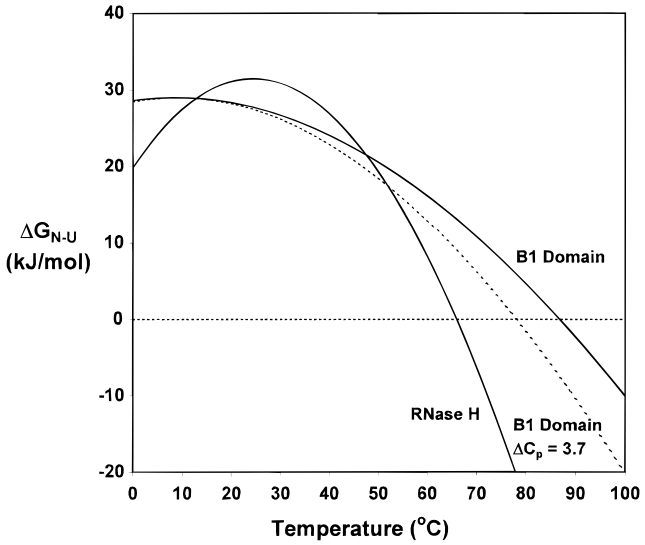

Fig. 6. Comparison of the thermal stability profiles for RNase H and the B1 domain. Solid lines correspond to the experimental values (Alexander et al., 1992a; Hollien & Marqusee, 1999). The dotted line is the simulated stability profile of the B1 domain with the heat capacity change upon unfolding ($\Delta C_{p,N-U}$) increased from 2.9 to 3.7 kJ/mol K but the enthalpy and entropy changes at 9 °C (the temperature of maximum stability) kept the same as the experimental values. These curves were generated according to Equation 1.

higher and lower temperatures due to the dramatically different curvature of the stability profiles. This curvature difference is a consequence of the different heat capacities of unfolding (see Equation 1; $\Delta C_{p,N-U}$ = 2.9 kJ/mol K for the B1 domain and 11.3 kJ/mol K for RNase H). The dominant contribution to $\Delta C_{p,N-U}$ is expected to be exposure of hydrophobic surfaces upon unfolding (Alexander et al., 1992a; Fersht, 1999). Thus, the 3.9-fold difference between the $\Delta C_{p,N-U}$ values for the B1 domain and RNase H primarily reflects the threefold difference in buried, nonpolar surface area of the two proteins (~2,900 and ~8,700 Å^2, respectively). Nevertheless, an additional contribution to $\Delta C_{p,N-U}$ may come from any changes in the conformational heat capacity of the protein chain that occur upon unfolding (Gomez et al., 1995). The current results indicate that the backbone heat capacity in secondary structure regions of the native B1 domain is higher than the heat capacity for comparable regions of RNase H and the E140Q calmodulin domain. Thus, the contribution to $\Delta C_{p,N-U}$ from backbone conformational fluctuations of the B1 domain is smaller than would be expected if the C_p values were similar to those in RNase H and the calmodulin domain. A rough estimate of the difference (~20 J/mol K residue) implies that the total heat capacity of the native B1 domain would be ~0.8 kJ/mol K lower if the secondary structure C_p values were similar to those in the other proteins; this estimate assumes that NH group motions of different residues are independent. This estimated change would increase $\Delta C_{p,N-U}$ to ~3.7 kJ/mol K, increasing the curvature of the stability profile and decreasing the denaturation temperature by ~9 °C, as illustrated by the dotted curve in Figure 6. Note that a change of similar magnitude (on a per residue basis) but in the opposite direction for RNase H would result in only a ~5 °C increase in T_m because of the steeper slope of the stability profile near the T_m (Fig. 6). Thus, variations in conformational heat capacity are most likely to have a noticeable influence on the denaturation temperatures of small proteins.

The current analysis indicates that an increase in the conformational heat capacity of backbone groups, manifested as an increase in the temperature sensitivity of backbone motions, may contribute a measurable amount to the high temperature stability of certain proteins. Intuitively, this effect may be understood by considering the temperature dependence of the backbone entropy. The relatively high heat capacities observed in the B1 domain indicate that secondary structure regions of this domain undergo relatively large increases in entropy upon an increase in temperature as compared with secondary structure regions of some other proteins. The higher entropy lowers the free energy of the native B1 domain, thus stabilizing the native structure at high temperatures. To our knowledge, this strategy for stabilization of thermophilic proteins has not been proposed previously. A large number of other mechanisms for stabilization of such proteins have been considered, including (Cowan, 1997): increasing intramolecular packing; increasing hydrogen bonds, salt bridges, and surface charge networks; increasing helix-forming amino acids; stabilization of helix dipoles; removal of flexible regions (surface loops and termini); and insertion of proline residues to limit the entropy of the unfolded state.

The present proposal that backbone entropy can stabilize the folded state appears at first to contradict the previous observation that removal of flexible regions can promote thermal stabilization of some proteins (Rice et al., 1996; Cowan, 1997). However, both in the case of the B1 domain and of flexible regions in other proteins, the entropy of these regions is lower in the native state than in the unfolded state. The difference is that formation of the B1 domain secondary and tertiary structure gives rise to favorable interactions such as hydrogen bonds and hydrophobic contacts that compensate for the loss of entropy; these interactions appear to be achievable without compete rigidification of the backbone. On the other hand, inclusion of flexible surface loops or terminal regions in proteins is generally not compensated by the formation of such favorable interactions so these regions tend to reduce the stability of the native structure.

Previously, it has been suggested that thermostable proteins have "anomalous rigidity" (Daniel et al., 1996; Jaenicke, 1996; Cowan, 1997). This contention appears in stark contrast to the present proposal that (at least in certain cases) they may have unusually high flexibility at high temperatures. The proposal that thermostable proteins are unusually rigid is based primarily on the observations of low hydrogen-deuterium (H-D) exchange rates (Wagner & Wuthrich, 1979) and low protease susceptibility (Jaenicke, 1996) of some thermostable proteins relative to their mesophilic analogs. However, the latter observations do not provide a reliable reflection of the small amplitude structural fluctuations that are detectable by the methods used in the present study. Both H-D exchange and protease susceptibility are likely to be dramatically enhanced (by several orders of magnitude) in unfolded or partially unfolded states relative to the native state. Therefore, measurements of these rates for apparently native proteins actually reflect the exchange rates in these nonnative states and the small proportion of time that the protein spends in these states (Wagner & Wuthrich, 1979; Milne et al., 1998). Slower rates for more stable proteins are a consequence of the smaller amount of time that the protein spends in the nonnative states, which is directly related to its thermal stability. Thus, it should be no surprise that higher stability correlates with lower H-D exchange or protease cleavage rates but these measurements should not be interpreted as reflecting increased small amplitude fluctuations of the folded state. In contrast, the relaxation properties of NH groups in native proteins are dominated by such fluctuations in the native state. Therefore, these relaxation methods provide a reliable approach to assessing native state flexibility.

Concluding remarks

The data presented here indicate that NH groups in the ordered secondary structure regions of the B1 domain make larger contributions to conformational heat capacity than those in similar regions of the two other proteins studied by these methods to date. The difference is estimated to contribute up to ~9 °C to the thermal denaturation temperature of the B1 domain. Thus, regulation of the backbone heat capacity of the native form of a protein appears to be a previously unrecognized mechanism to control the stability of thermostable proteins. This mechanism is expected to be most effective for small proteins whose total heat capacity is small resulting in relatively low curvature of their stability profiles (Fig. 6). However, it is important to recognize that this effect is subtle and exists within the background of many other contributions to protein stability. Thus, separation of the backbone entropy term from other terms is only possible through the use of methods, such as ^{15}N NMR relaxation, that are selectively sensitive to backbone motions. Recent studies have indicated that increases in protein conformational entropy upon ligand binding may help to stabilize protein–ligand complexes (Farrow et al., 1994; Stivers et al., 1996; Yu et al., 1996; Zidek et al., 1999). Taken together with the present results, these studies suggest that regulation of

protein entropy may be a rather widespread, albeit subtle, mechanism contributing to a variety of biochemical equilibrium processes.

Materials and methods

Protein expression and purification

All experiments used the B1 domain containing the T2Q mutation that prevents processing of the N-terminal methionine residue; expression of wild-type protein yields a mixture of processed and unprocessed material (Smith et al., 1994). Uniformly ^{15}N-labeled B1 domain was expressed in *Escherichia coli* using an expression vector derived from pET11 (Novagen, Madison, Wisconsin) (Smith et al., 1994). BL21(DE3) *E. coli* cells transformed with the expression vector were grown in minimal media (Stone et al., 1995) containing 3.0 g/L glucose, 0.5 g/L $^{15}NH_4Cl$, and 0.5 g/L $(^{15}NH_4)_2SO_4$ at 37 °C to an optical density (550 nm) of ~0.8. Isopropyl-β-D-thiogalactopyranoside was added to a final concentration of 1 mM and growth was continued for 4 h. Cells were collected by centrifugation, suspended in 20 mM Tris, pH 8, and lysed by sonication. Phenylmethylsulfonyl fluoride (PMSF) was added to a final concentration of 1 mM, cells were warmed to 80 °C in a water bath for 5 min, and the PMSF concentration was increased to 2 mM. The mixture was stirred for 30 min then centrifuged for 30 min at 12,000 rpm. The supernatant was treated with poly(ethyleneimine) (final concentration 0.4%) to precipitate nucleic acids and passed through a 0.2 μm filter then loaded onto a 15Q-Sepharose anion exchange column (Pharmacia Biotech, Piscataway, New Jersey) pre-equilibrated with 20 mM Tris, pH 8, and eluted with a NaCl gradient. The B1 domain eluted at 200 mM NaCl and was further purified by size exclusion chromatography using a HiLoad 16/60 Superdex 75 column (Pharmacia Biotech). The protein concentration was determined by absorbance at 280 nm (ϵ_{280} = 9,530 L mol^{-1} cm^{-1} calculated from the amino acid sequence).

NMR measurements

NMR experiments were performed using a sample of 2.7 mM uniformly ^{15}N-labeled B1 domain dissolved in 50 mM phosphate, 0.02% NaN_3, H_2O/D_2O (90/10), pH 5.2. R_1 and R_2 experiments at 50 °C were repeated using a 0.9 mM sample in the same buffer. Experiments were performed on a Varian UnityINOVA 500 MHz NMR spectrometer equipped with three radiofrequency channels, pulsed field gradients, and a ^{1}H-detect triple resonance (HCN) probe. The probe temperature was calibrated using external standards of neat methanol (0–20 °C) or ethylene glycol (30–50 °C). Chemical shifts were referenced to the 0 ppm proton signal of an external DSS standard (Wishart et al., 1995).

Except where otherwise noted, all experiments were recorded at each of six temperatures: 0, 10, 20, 30, 40, and 50 °C. The ^{1}H carrier was placed on the water resonance and the ^{15}N carrier was placed at 120 ppm. Experiments were performed using gradient sensitivity enhancement (Kay et al., 1992), and ^{15}N decoupling was performed during acquisition using a 1.25 kHz GARP sequence. All two-dimensional (2D) experiments were performed using 128 and 2,048 complex points and spectral widths of 2,000 and 7,000 Hz in ^{15}N and ^{1}H dimensions, respectively, and eight transients per FID. The ^{15}N longitudinal relaxation rate constant (R_1), the ^{15}N transverse relaxation rate constant (R_2), and the heteronuclear $\{^1H\}-^{15}N$ NOE were each measured using published 2D ^{1}H-^{15}N HSQC-style pulse sequences (Farrow et al., 1994; Kroenke et al., 1998). For R_1 and R_2 experiments, the relaxation delay τ was varied among eight different values; experiments at four of these values were duplicated to allow estimation of peak height uncertainties. Delay values used were τ = 11*, 55, 133, 233*, 377, 555*, 888, and 1,998* ms for the R_1 experiment and τ = 17*, 33, 67*, 100, 150, 200*, 283, and 383* ms for the R_2 experiment; asterisks indicate duplicated points. For R_1 and R_2 experiments, the recycle delay was 2 s. Four identical pairs of $\{^1H\}-^{15}N$ NOE experiments were recorded at each temperature. In one experiment of each pair, protons were saturated throughout the 5 s recycle delay by application of 120° pulses (field strength 10 kHz) spaced 5 ms apart; in the other experiment, a 5 s recycle delay was used without proton saturation. In theory, NOE values measured in this way may contain a small systematic error due to chemical exchange with saturated solvent protons during the experiment without ^{1}H saturation (Kay et al., 1989; Clore et al., 1990a; Stone et al., 1992). Assuming a water T_1 of 4.5 s (Stone et al., 1993), up to 20% water saturation, and an amide exchange rate of greater than ~1 s^{-1}, this effect will result in a systematic increase of up to 7% in the apparent NOE; smaller increases will occur if the N–H group is protected from exchange with solvent. Model calculations showed that the effect of this systematic error on dynamics parameters is negligible. The ^{15}N transverse cross-relaxation rate constant (η_{xy}) was recorded using the pulse sequence of Kroenke et al. (1998) in which antiphase ^{15}N magnetization ($2N_yH_z$) is created and allowed to cross-relax with in-phase (N_y) magnetization for a time τ. The component that converted to N_y and the component that remained as $2N_yH_z$ were detected in consecutively recorded experiments at each of six different delay values; experiments at three of these values were duplicated to allow uncertainties to be estimated. Delays used were τ = 22*, 43, 65*, 76, 98, and 109* ms; asterisks indicate duplicated points. The recycle delay was 1.5 s. Three-dimensional TOCSY-HSQC and NOESY-HSQC experiments, for resonance assignments, were recorded at 0, 20, and 50 °C using published pulse sequences (Zhang et al., 1994) with mixing times of 52 and 100 ms, respectively. TOCSY transfer was achieved using a DIPSI-2rc isotropic mixing sequence (Cavanagh & Rance, 1992). Both experiments were performed using 96, 32, and 2,048 complex points and spectral widths of 6,000, 2,000, and 7,000 Hz in the ω_1 (^{1}H), ω_2 (^{15}N), and ω_3 (^1H_N) dimensions, respectively, four transients per FID and a recycle delay of 1.5 s. Approximate times required for recording the data at each temperature were 20 h (R_1), 17 h (R_2), 31 h (NOE), 20 h (η_{xy}), 26 h (TOCSY-HSQC), and 26.5 h (NOESY-HSQC).

Determination of relaxation parameters

NMR data were processed using Felix 95 (Molecular Simulations, Inc., Burlington, Massachusetts) running on Silicon Graphics O2 workstations. All spectra were processed using 2–3 Hz line broadening in the direct dimension, cosine bell window functions in indirect dimensions, a lowpass filter to suppress the solvent signal, and polynomial baseline correction. Intensities (heights) of peaks in the 2D spectra were measured using macros provided with the Modelfree 3.1 program (Palmer et al., 1991), modified slightly to be compatible with Felix 95. In the case of doublet peaks, exhibiting resolved ^{1}H–^{1}H couplings, the intensity was taken as the average of the peak heights measured separately for each compo-

nent. Uncertainties in peak heights were estimated from the duplicate experiments. For time points that were repeated in the R_1, R_2, and η_{xy} experiments, the differences in peak heights between the duplicate spectra were determined. The absolute uncertainty in the peak heights (assumed to be the same for all peaks) was taken to be the standard deviation of the differences divided by $\sqrt{2}$. For other time points in these experiments, the absolute uncertainty in the peak heights was determined by linear interpolation between the duplicated points. R_1 and R_2 values were obtained from weighted fits of the intensity as a function of the relaxation time to a single exponential function decaying to zero. The transverse cross-relaxation rate constant η_{xy} was obtained from a weighted fit of the intensity $I(\tau)$ as a function of the relaxation time τ to the equation (Kroenke et al., 1998):

$$I_{\text{cross}}/I_{\text{auto}} = \tanh(\eta_{xy}\tau) \tag{2}$$

in which τ is the relaxation period, and I_{cross} and I_{auto} are the peak heights in the experiments detecting the S_y and $2I_zS_y$ coherences, respectively. The relative uncertainty in the ratio $I_{\text{cross}}/I_{\text{auto}}$ was taken to be the sum of the relative uncertainties in I_{cross} and I_{auto}. Steady-state NOEs were calculated from the ratios of the cross-peak heights in the presence (I_{sat}) and the absence (I_{unsat}) of proton saturation during the recycle delay (NOE = I_{sat}/I_{unsat}). The NOE for each NH group at each temperature was calculated separately from each of the four repeated pairs of experiments. The NOE was taken to be the average of the four measurements. Using the standard deviation of the four measurements as the NOE uncertainty would result in severe underestimation of the true uncertainty for several residues and therefore to unrealistic weighting of the NOE in subsequent model-free dynamics calculations. Thus, we have made the assumption that the absolute uncertainty in the NOE is the same for all residues at a given temperature. This uncertainty was then taken as the average of the standard deviation values determined separately for each residue from the four data sets.

Estimation of the molecular diffusion tensor and identification of residues undergoing slow exchange

An initial estimate of the dimensions and orientation of the diffusion tensor at each temperature was obtained from the ratios of ^{15}N R_2 and R_1 values. The fitting procedure has been described previously (Tjandra et al., 1995) and was implemented as a systematic grid search in the program quadric diffusion, provided by Dr. A.G. Palmer III (Columbia University, New York). Residues with large amplitude fast internal motions (NOE $\leq$ 0.3) were excluded from the calculation. Among the remaining residues, those with significant conformational exchange on the microsecond–millisecond timescale were also excluded, based on the criterion that their R_2/η_{xy} values exceeded the average ratio at that temperature by more than one standard deviation. This criterion is based upon the following relationship that was derived under the assumption that R_2 is dominated by low frequency spectral densities [i.e., $4J(0) + 3J(\omega_N) \gg J(\omega_H - \omega_N) + 6J(\omega_H) + 6J(\omega_H + \omega_N)$] (Fushman & Cowburn, 1998):

$$R_2/\eta_{xy} \approx \frac{(d^2/8 + c^2/6)[4J(0) + 3J(\omega_N)] + R_{ex}}{(-\sqrt{3}/6)cdP_2(\cos\beta)[4J(0) + 3J(\omega_N)]}. \tag{3}$$

In Equation 3, $J(\omega)$ is the spectral density function at frequency ω; $c = (\omega_N/\sqrt{3})(\Delta\sigma)$ and $d = [\mu_0 h\gamma_N\gamma_H/(8\pi^2)] < (1/r_{NH})^3 >$; $\Delta\sigma = -170$ ppm is the chemical shift anisotropy (CSA) of ^{15}N nuclei in helical polypeptide chains (Tjandra et al., 1996); μ_0 is the permeability of vacuum; h is Planck's constant; γ_N and γ_H are the gyromagnetic ratios of ^{1}H and ^{15}N, respectively; $r_{NH} = 1.02$ Å is the length of the amide bond vector; β is the angle between the unique axis of the CSA and dipolar tensors [20–24° for an NH group participating in a peptide bond (Hiyama et al., 1988)]; $P_2(x) = (3x^2 - 1)/2$; and R_{ex} is the contribution to R_2 of conformational or chemical exchange on the microsecond–millisecond timescale (Palmer et al., 1996). In the absence of an R_{ex} contribution, the spectral density terms in Equation 3 cancel and the ratio is expected to be approximately constant for all NH groups, as long as r_{NH}, $\Delta\sigma$, and β do not vary significantly. NH groups, whose transverse relaxation rates include an R_{ex} contribution, will display significantly increased R_2/η_{xy} ratios. Although the method used here yields only a qualitative indication of residues with R_{ex} contributions, it has the advantages over alternative methods (Szyperski et al., 1993; Farrow et al., 1995; Peng & Wagner, 1995; Phan et al., 1996; Akke et al., 1998; Kroenke et al., 1998) that it requires only a single relaxation parameter (η_{xy}) to be measured at a single field strength, data collection is achieved in a comparable time to the other relaxation measurements (~20 h at each temperature in the present study), and analysis of the data is straightforward. For the model-free fits described below, the shape and orientation of the diffusion tensor were kept constant for all temperatures (see Results).

Calculation of model-free dynamics parameters

The R_1, R_2, and NOE are dependent on the spectral densities $J(\omega)$ at five frequencies (Lipari & Szabo, 1982a). The R_2 may also include a contribution (R_{ex}) from conformational exchange on the microsecond–millisecond timescale (Palmer et al., 1996). In the current study, the relaxation parameters were fitted to extended versions of the Lipari–Szabo model-free dynamics formalism (Lipari & Szabo, 1982a, 1982b), in which the spectral density $J(\omega)$ is defined as a function of the rotational diffusion tensor for the whole molecule and three or fewer internal dynamics parameters for each NH group. Substitution of $J(\omega)$ into the expressions for the relaxation parameters allows the three measured relaxation parameters to be written as functions of the same dynamics variables; thus, nonlinear fitting allows the dynamics parameters to be calculated that agree most closely with the measured relaxation parameters. The models used here incorporated an axially symmetric diffusion tensor (Barbato et al., 1992) and, in some cases, two timescales of internal motions (Clore et al., 1990a, 1990b). The models are described by the following general equation (Barbato et al., 1992) or simplified versions thereof:

$$J(\omega) = \frac{2}{5}S_a^2\sum_{j=1}^{3}A_j\left[\frac{S_b^2\tau_m}{1 + (\omega\tau_m)^2} + \frac{\tau_j'(1 - S_b^2)}{1 + (\omega\tau_j')^2}\right] \tag{4}$$

in which $S^2 = S_a^2S_b^2$ is the square of the generalized order parameter characterizing the amplitude of the internal motions; S_a^2 and S_b^2 are the squares of the order parameters for internal motions on the specific timescales described below for each model; $\tau_m = (2D_{\|} + 4D_{\perp})^{-1}$ is the effective overall correlation time; $\tau_j' = \tau_j\tau_e/(\tau_j + \tau_e)$; τ_e is the effective internal correlation time for motions on the timescale described below for each model; $\tau_1^{-1} = 6D_{\perp}$; $\tau_2^{-1} = 5D_{\perp} + D_{\|}$; $\tau_3^{-1} = 2D_{\perp} + 4D_{\|}$; $D_{\|}$ and $D_{\perp}$ are the diffusion constants

for rotation around the unique and perpendicular axes, respectively; $A_1 = (3\cos^2\theta - 1)^2/4$; $A_2 = 3\sin^2\theta\cos^2\theta$; $A_3 = (3/4)\sin^4\theta$; and θ is the angle between the N–H bond vector and the unique axis of the principal frame of the diffusion tensor.

Five different models were used to characterize the internal dynamics of N–H groups, the most complex of which is shown in Equation 4. Fitting the relaxation data to each model requires optimization of one or more of the following internal motional parameters: S_a^2, S_b^2, τ_e, and R_{ex}. Model 1 (Lipari & Szabo, 1982a, 1982b) describes NH groups exhibiting only a single very fast timescale ($\lesssim$20 ps) of internal motion. S_b^2 is optimized and is redefined as S_f^2, the square of the order parameter for fast internal motions. It is assumed that $S_a^2 \sim 1$, $\tau_e \sim 0$, and $R_{ex} \sim 0$. Model 2 (Lipari & Szabo, 1982a, 1982b) is equivalent to model 1 except that τ_e (redefined as τ_f) is now in the timescale ~20–500 ps. S_f^2 and τ_f are optimized; the assumptions that $S_a^2 \sim 1$ and $R_{ex} \sim 0$ are retained. Models 3 and 4 are equivalent to models 1 and 2, respectively, except that the R_{ex} term is now optimized in addition to the other parameters (Clore et al., 1990a; Palmer et al., 1991; Stone et al., 1992). Finally, model 5 (Clore et al., 1990a, 1990b) describes internal motions on two timescales faster than the overall correlation time. S_a^2 is redefined as S_f^2, the square of the order parameter for very fast internal motions (assumed to be faster than ~20 ps), S_b^2 is redefined as S_s^2, the square of the order parameter for internal motions slower than ~500 ps, and τ_e is redefined as τ_s, the timescale for slower internal motions ($\tau_s \geq 500$ ps). R_{ex} is assumed to be zero. This model is described by Equation 4 in which S_f^2, S_s^2, and τ_e are substituted by S_f^2, S_s^2, and τ_s, respectively.

Model-free calculations were performed using the program Modelfree version 4.0, provided by A.G. Palmer III (Columbia University, New York). Model selection for each residue was performed according to the flowchart outlined by Mandel et al. (1995). This procedure identified models to adequately describe the relaxation data for 49–52 residues at each temperature. To utilize all measured relaxation parameters, N–H groups that were excluded by the model selection flowchart were fit to the three-parameter model (model 4 or 5) yielding the lower χ^2 value. If the calculated parameters allowed for a simplification of the three-parameter model (e.g., $R_{ex} = 0$), then the simplified model (e.g., model 2) was chosen. This alternative model selection procedure was required for only four residues at 0 °C (two fit to model 3 and two fit to model 5), one residue at 10 °C (fit to model 5), four residues at 20 °C (three fit to model 3 and one fit to model 5), two residues at 30 °C (one fit to model 1 and one fit to model 5), no residues at 40 °C, and two residues at 50 °C (one fit to model 2 and one fit to model 5). Uncertainties in the dynamics parameters were determined using Monte Carlo simulations carried out by the Modelfree program (Palmer et al., 1991; Stone et al., 1992).

Calculation of heat capacities and characteristic temperatures

The entropy (S_B) associated with angular fluctuations of each NH group at each temperature was calculated from the order parameter according to the equation (Yang & Kay, 1996; Evenäs et al., 1999):

$$S_B = k_B \cdot \ln[\pi \cdot (3 - \sqrt{(1 + 8 \cdot S)})] \quad (5)$$

in which S is the generalized order parameter and k_B is Boltzmann's constant. Equation 5 was derived according to the diffusion-in-a-cone model of NH group motions under the assumption that the motions of individual NH groups are independent of each other. The local heat capacity for each NH group was then calculated as the slope of a linear fit of entropy vs. the natural logarithm of the temperature (Yang et al., 1997; Evenäs et al., 1999) according to the equation:

$$C_p = \frac{dS_B}{d\ln(T)}. \quad (6)$$

The characteristic temperature (T^*) for each NH group, indicating the density of energy states accessible upon an increase in temperature, was calculated from the slope of a linear fit of $(1 - S)$ vs. temperature according to the equation (Mandel et al., 1996):

$$\frac{3}{2T^*} = \frac{d(1 - S)}{dT} \quad (7)$$

which was derived under the assumption that the NH groups undergo only small excursions within an axially symmetric parabolic potential.

Solvent accessible surface area (SASA) measurements were made using the program NACCESS (S.J. Hubbard & J.M. Thornton, University College, London).

Supplementary material in the Electronic Appendix

Six tables containing relaxation data (R_1, R_2, NOE, and η_{xy}) at 0, 10, 20, 30, 40, and 50 °C, and six tables containing model-free data (S_f^2, S_s^2, τ_e, and R_{ex}) at 0, 10, 20, 30, 40, and 50 °C.

Acknowledgments

The authors thank Drs. Arthur G. Palmer III (Columbia University), Mark Rance (University of Cincinnati), and Mikael Akke (Lund University) for many helpful discussions and for providing data processing programs and Drs. Rance and Lewis E. Kay (University of Toronto) for providing pulse programs. This work was supported by grants from the National Science Foundation (MCB-9600968 to M. Stone and MCB-9316863 to L.R.) and from the National Institutes of Health (GM-55055 to M. Stone and GM-57265 to L.R.). Acknowledgment is made to the donors of The Petroleum Research Fund, administered by the American Chemical Society, for partial support of this research (M. Stone). L.R. is a Dreyfus Teacher-Scholar. M. Seewald was supported by a Bayreuth University-Indiana University Graduate Exchange Fellowship.

References

Achari A, Hale SP, Howard AJ, Clore GM, Gronenborn AM, Hardman KD, Whitlow M. 1992. 1.67-Å X-ray structure of the B2 immunoglobulin-binding domain of Streptococcal protein G and comparison to the NMR structure of the B1 domain. *Biochemistry 31*:10449–10457.

Akerstrom B, Brodin T, Reis K, Bjorck L. 1985. Protein G: A powerful tool for binding and detection of monoclonal and polyclonal antibodies. *J Immunol 135*:2589–2592.

Akke M, Bruschweiler R, Palmer AG III. 1993. NMR order parameters and free energy: An analytical approach and its application to cooperative Ca^{2+} binding by calbindin D_{9k}. *J Am Chem Soc 115*:9832–9833.

Akke M, Liu J, Cavanagh J, Erickson HP, Palmer AG. 1998. Pervasive conformational fluctuations on microsecond time scales in a fibronectin type III domain. *Nat Struct Biol 5*:55–59.

Alexander P, Fahnestock S, Lee T, Orban J, Bryan P. 1992a. Thermodynamic analysis of the folding of the Streptococcal protein G IgG-binding domains B1 and B2: Why small proteins tend to have high denaturation temperatures. *Biochemistry 31*:3597–3603.

Alexander P, Orban J, Bryan P. 1992b. Kinetic analysis of folding and unfolding the 56 amino acid IgG-binding domain of Streptococcal protein G. *Biochemistry 31*:7243–7248.

Barbato G, Ikura M, Kay LE, Pastor RW, Bax A. 1992. Backbone dynamics of calmodulin studied by ^{15}N relaxation using inverse detected two-dimensional NMR spectroscopy: The central helix is flexible. *Biochemistry 31*:5269–5278.

Barchi JJ, Grasberger B, Gronenborn AM, Clore GM. 1994. Investigation of the backbone dynamics of the IgG-binding domain of streptococcal protein G by heteronuclear two-dimensional ^{1}H-^{15}N nuclear magnetic resonance spectroscopy. *Protein Sci 3*:15–021.

Bhattacharya S, Falzone C, Lecomte J. 1999. Backbone dynamics of apocytochrome b5 in its native, partially folded state. *Biochemistry 38*:2577–2589.

Bjorck L, Kronvall G. 1984. Purification and some properties of Streptococcal protein G, a novel IgG-binding reagent. *J Immunol 133*:969–974.

Blackledge M, Cordier F, Dosset P, Marion D. 1998. Precision and uncertainties in the characterization of anisotropic rotational diffusion by ^{15}N relaxation. *J Am Chem Soc 120*:4538–4539.

Blanco FJ, Serrano L. 1998. Folding of protein G B1 domain studied by the conformational characterization of fragments comprising its secondary structure elements. *Eur J Biochem 230*:634–649.

Boyle M. 1990. *Bacterial immunoglobulin-binding proteins*. San Diego, CA: Academic Press.

Bracken C, Carr PA, Cavanagh J, Palmer AG III. 1999. Temperature dependence of intramolecular dynamics of the basic leucine zipper of GCN4: Implications for the entropy of association with DNA. *J Mol Biol 285*:2133–2146.

Cavanagh J, Rance M. 1992. Suppression of cross-relaxation effects in TOCSY spectra via a modified DIPSI-2 mixing sequence. *J Mag Reson 96*:670–678.

Clore GM, Driscoll PC, Wingfield PT, Gronenborn AM. 1990a. Analysis of the backbone dynamics of interleukin-1β using two-dimensional inverse detected heteronuclear ^{15}N-^{1}H NMR spectroscopy. *Biochemistry 29*:7387–7401.

Clore GM, Szabo A, Bax A, Kay LE, Driscoll PC, Gronenborn AM. 1990b. Deviations from the simple two-parameter model-free approach to the interpretation of nitrogen-15 nuclear magnetic relaxation of proteins. *J Am Chem Soc 112*:4989–4991.

Cowan DA. 1997. Thermophilic proteins: Stability and function in aqueous and organic solvents. *Comp Biochem Physiol A 118*:429–438.

Creighton TE. 1993. *Proteins: Structure and molecular properties*. New York: W.H. Freeman and Company.

Dahiyat BI, Mayo SL. 1998. Probing the role of packing specificity in protein design. *Proc Natl Acad Sci USA 94*:10172–10177.

Daniel R, Dines M, Petach H. 1996. The denaturation and degradation of stable enzymes at high temperatures. *Biochem J 317*:1–11.

Evenäs J, Forsén S, Malmendal A, Akke M. 1999. Backbone dynamics and energetics of a calmodulin domain mutant exchanging between closed and open conformations. *J Mol Biol 289*:603–617.

Fahnestock S, Alexander P, Fipula D, Nagle J. 1990. Structure and evolution of the Streptococcal genes encoding protein G. In: Boyle MDP, ed. *Bacterial immunoglobulin-binding proteins*. San Diego, CA: Academic Press. pp 133–148.

Farrow NA, Muhandiram R, Singer AU, Pascal SM, Kay CM, Gish G, Shoelson SE, Pawson T, Forman-Kay JD, Kay LE. 1994. Backbone dynamics of a free and a phosphopeptide-complexed Src homology 2 domain studied by ^{15}N NMR relaxation. *Biochemistry 33*:5984–6003.

Farrow NA, Zhang OW, Formankay JD, Kay LE. 1997. Characterization of the backbone dynamics of folded and denatured states of an SH3 domain. *Biochemistry 36*:2390–2402.

Farrow NA, Zhang OW, Szabo A, Torchia DA, Kay LE. 1995. Spectral density function mapping using N-15 relaxation data exclusively. *J Biomol NMR 6*:153–162.

Fersht A. 1999. *Structure and mechanism in protein science*. New York: W.H. Freeman and Company.

Frank MK, Clore GM, Gronenborn AM. 1995. Structural and dynamic characterization of the urea denatured state of the immunoglobulin binding domain of Streptococcal protein G by multidimensional heteronuclear NMR spectroscopy. *Protein Sci 4*:2605–2615.

Fushman D, Cowburn D. 1998. Model-independent analysis of ^{15}N chemical shift anisotropy from NMR relaxation data. Ubiquitin as a test example. *J Am Chem Soc 120*:7109–7110.

Gallagher T, Alexander P, Bryan P, Gilliland GL. 1994. Two crystal structures of the B1 immunoglobulin-binding domain of Streptococcal protein G and comparison with NMR. *Biochemistry 33*:4721–4729.

Gomez J, Hilser V, Xie D, Freire E. 1995. The heat capacity of proteins. *Proteins Struct Funct Genet 22*:404–412.

Gronenborn AM, Filpula DR, Essig NZ, Achari A, Whitlow M, Wingfield PT, Clore GM. 1991. A novel, highly stable fold of the immunoglobulin binding domain of Streptococcal protein G. *Science 253*:657–661.

Gronenborn AM, Frank MK, Clore GM. 1996. Core mutants of the immunoglobulin binding domain of streptococcal protein G: Stability and structural integrity. *FEBS Lett 398*:312–316.

Hiyama Y, Niu C-H, Silverton JV, Bavoso A, Torchia DA. 1988. Determination of ^{15}N chemical shift tensor via ^{15}N-^{2}H dipolar coupling in Boc-glycylglycyl[^{15}N]glycine benzyl ester. *J Am Chem Soc 110*:2378–2383.

Hollien J, Marqusee S. 1999. A thermodynamic comparison of mesophilic and thermophilic ribonucleases H. *Biochemistry 38*:3831–3836.

Jaenicke R. 1996. Glyceraldehyde-3-phosphate dehydrogenase from *Thermotoga maritima*: Strategies of protein stabilization. *FEMS Microbiol Rev 18*:215–224.

Jin C, Liao X. 1999. Backbone dynamics of a winged helix protein and its DNA complex at different temperatures: Changes of internal motions in Genesis upon binding to DNA. *J Mol Biol 292*:641–651.

Jin D, Andrec M, Montelione GT, Levy RM. 1998. Propagation of experimental uncertainties using the Lipari-Szabo model-free analysis of protein dynamics. *J Biomol NMR 12*:471–492.

Kay LE, Keifer P, Saarinen T. 1992. Pure absorption gradient enhanced heteronuclear single quantum correlation spectroscopy with improved sensitivity. *J Am Chem Soc 114*:10663–10665.

Kay LE, Torchia DA, Bax A. 1989. Backbone dynamics of proteins as studied by ^{15}N inverse detected heteronuclear NMR spectroscopy: Application to Staphylococcal nuclease. *Biochemistry 28*:8972–8979.

Kobayashi N, Honda S, Yoshii H, Uedaira H, Munekata E. 1995. Complement assembly of two fragments of the streptococcal protein G B1 domain in aqueous solution. *FEBS Lett 366*:99–103.

Kroenke CD, Loria JP, Lee LK, Rance M, Palmer AG. 1998. Longitudinal and transverse ^{1}H-^{15}N dipolar/^{15}N chemical shift anisotropy relaxation interference: Unambiguous determination of rotational diffusion tensors and chemical exchange effects in biological macromolecules. *J Am Chem Soc 120*:7905–7915.

Kuszewski J, Clore GM, Gronenborn AM. 1994. Fast folding of a prototypic polypeptide: The immunoglobulin binding domain of Streptococcal protein G. *Protein Sci 3*:1945–1952.

Li Z, Raychaudhuri S, Wand AJ. 1996. Insights into the local residual entropy of proteins provided by NMR relaxation. *Protein Sci 5*:2647–2650.

Lipari G, Szabo A. 1980. Effect of librational motions on fluorescence depolarization and nuclear magnetic resonance relaxation in macromolecules and membranes. *Biophys J 30*:489–506.

Lipari G, Szabo A. 1981. Pade approximants to correlation functions for restricted rotational diffusion. *J Chem Phys 75*:2971–2976.

Lipari G, Szabo A. 1982a. Model-free approach to the interpretation of nuclear magnetic resonance relaxation in macromolecules. 1. Theory and range of validity. *J Am Chem Soc 104*:4546–4559.

Lipari G, Szabo A. 1982b. Model-free approach to the interpretation of nuclear magnetic resonance relaxation in macromolecules. 2. Analysis of experimental results. *J Am Chem Soc 104*:4559–4570.

Mandel AM, Akke M, Palmer AG. 1996. Dynamics of ribonuclease H: Temperature dependence of motions on multiple time scales. *Biochemistry 35*:16009–16023.

Mandel AM, Akke M, Palmer AG III. 1995. Backbone dynamics of *Escherichia coli* ribonuclease HI: Correlations with structure and function in an active enzyme. *J Mol Biol 246*:144–163.

Meekhof A, Freund S. 1999. Probing residual structure and backbone dynamics on the milli- to picosecond timescale in a urea-denatured Fibronectin type III domain. *J Mol Biol 286*:579–592.

Milne JS, Mayne L, Roder H, Wand AJ, Englander SW. 1998. Determinants of protein hydrogen exchange studied in equine cytochrome c. *Protein Sci 7*:739–745.

Minor DL, Kim PS. 1994a. Measurement of the β-sheet-forming propensities of amino acids. *Nature 367*:660–663.

Minor DL, Kim PS. 1994b. Context is a major determinant of β-sheet propensity. *Nature 371*:264–267.

Minor DL, Kim PS. 1996. Context-dependent secondary structure formation of a designed protein sequence. *Nature 380*:730–734.

O'Neil KT, Hoess RH, Raleigh DP, DeGrado WF. 1995. Thermodynamic genetics of the folding of the B1 immunoglobulin-binding domain from Streptococcal protein G. *Proteins Struct Funct Genet 21*:11–21.

Orban J, Alexander P, Bryan P. 1994. Hydrogen-deuterium exchange in the free and immunoglobulin G-bound protein G B-domain. *Biochemistry 33*:5702–5710.

Orban J, Alexander P, Bryan P, Khare D. 1995. Assessment of stability differences in the protein G B1 and B2 domains from hydrogen-deuterium exchange: Comparison with calorimetric data. *Biochemistry 34*:15291–15300.

Palmer AG, Williams J, Mcdermott A. 1996. Nuclear magnetic resonance studies of biopolymer dynamics. *J Phys Chem 100*:13293–13310.

Palmer AG III, Rance M, Wright PE. 1991. Intramolecular motions of a zinc finger DNA-binding domain from Xfin characterized by proton-detected natural abundance ^{13}C heteronuclear NMR spectroscopy. *J Am Chem Soc 113*:4371–4380.

Park S-H, O'Neil KT, Roder H. 1997. An early intermediate in the folding reaction of the B1 domain of protein G contains a native-like core. *Biochemistry 36*:14277–14283.

Peng JW, Wagner G. 1995. Frequency spectrum of NH bonds in eglin c from spectral density mapping at multiple fields. *Biochemistry 34*:16733–16752.

Phan IQH, Boyd J, Campbell ID. 1996. Dynamic studies of a fibronectin type I module pair at three frequencies: Anisotropic modelling and direct determination of conformational exchange. *J Biomol NMR 8*:369–378.

Rice D, Yip K, Stillman T, Britton K, Fuentes A, Connerton I, Pasquo A, Scandurra R, Engel P. 1996. Insights into the molecular basis of thermal stability from the structure determination of Pyrococus furiosus glutamate dehydrogenase. *FEMS Microbiol Rev 18*:105–117.

Sanders JKM, Hunter BK. 1987 *Modern NMR spectroscopy*. New York: Oxford University Press.

Sheinerman FB, Brooks CL. 1998. Calculations on folding of segment B1 of Streptococcal protein G. *J Mol Biol 278*:439–456.

Smith CK, Regan L. 1995. Guidelines for protein design: The energetics of β-sheet side chain interactions. *Science 270*:980–982.

Smith CK, Withka JM, Regan L. 1994. A thermodynamic scale for the β-sheet forming tendencies of the amino acids. *Biochemistry 33*:5510–5517.

Stivers JT, Abeygunawardana C, Mildvan AS. 1996. ^{15}N NMR relaxation studies of free and inhibitor-bound 4-oxalocrotonate tautomerase: Backbone dynamics and entropy changes of an enzyme upon inhibitor binding. *Biochemistry 35*:16036–16047.

Stone MJ, Chandrasekhar K, Holmgren A, Wright PE, Dyson HJ. 1993. Comparison of backbone and tryptophan side-chain dynamics of reduced and oxidized *Escherichia coli* thioredoxin using ^{15}N NMR relaxation measurements. *Biochemistry 32*:426–435.

Stone MJ, Fairbrother WJ, Palmer AG III, Reizer J, Saier MH Jr, Wright PE. 1992. Backbone dynamics of the *Bacillus subtilis* glucose permease IIA domain determined from ^{15}N NMR relaxation measurements. *Biochemistry 31*:4394–4406.

Stone MJ, Ruf W, Miles DJ, Edgington TS, Wright PE. 1995. Recombinant soluble human tissue factor secreted by *Saccharomyces cerevisiae* and refolded from *Escherichia coli* inclusion bodies: Glycosylation of mutants, activity and physical characterization. *Biochem J 310*:605–614.

Szyperski T, Luginbühl P, Otting G, Güntert P, Wüthrich K. 1993. Protein dynamics studied by rotating frame ^{15}N spin relaxation times. *J Biomol NMR 3*:151–164.

Tjandra N, Feller SE, Pastor RW, Bax A. 1995. Rotational diffusion anisotropy of human ubiquitin from N-15 NMR relaxation. *J Am Chem Soc 117*:12562–12566.

Tjandra N, Szabo A, Bax A. 1996. Protein backbone dynamics and N-15 chemical shift anisotropy from quantitative measurement of relaxation interference effects. *J Am Chem Soc 118*:6986–6991.

Wagner G, Wuthrich K. 1979. Correlation between the amide proton exchange rates and the denaturation temperatures in globular proteins related to the basic pancreatic trypsin inhibitor. *J Mol Biol 130*:31–37.

Wishart DS, Bigam CG, Yao J, Abildgaard F, Dyson HJ, Oldfield E, Markley JL, Sykes BD. 1995. ^{1}H, ^{13}C and ^{15}N chemical shift referencing in biomolecular NMR. *J Biomol NMR 6*:135–140.

Yang D, Kay LE. 1996. Contributions to conformational entropy arising from bond vector fluctuations measured from NMR-derived order parameters: Application to protein folding. *J Mol Biol 263*:369–382.

Yang D, Yu-Keung M, Forman-Kay JD, Farrow NA, Kay LE. 1997. Contributions to protein entropy and heat capacity from bond vector motions measured by NMR spin relaxation. *J Mol Biol 272*:790–804.

Yu L, Zhu CX, Tse-Dinh YC, Fesik SW. 1996. Backbone dynamics of the C-terminal domain of *Escherichia coli* topoisomerase I in the absence and presence of single-stranded DNA. *Biochemistry 35*:9661–9666.

Zhang O, Kay LE, Olivier JP, Forman-Kay JD. 1994. Backbone ^{1}H and ^{15}N resonance assignments of the N-terminal SH3 domain of drk in folded and unfolded states using enhanced-sensitivity pulsed field gradient NMR techniques. *J Biomol NMR 4*:845–858.

Zidek L, Novotny MV, Stone MJ. 1999. Increased protein backbone conformational entropy upon hydrophobic ligand binding. *Nat Struct Biol 6*:1118–1121.